



CrossMark  
click for updates

Cite this: *RSC Adv.*, 2015, 5, 4219

## Photophysical property vs. medium: mononuclear, dinuclear and trinuclear Zn(II) complexes†

Amar Hens and Kajal Krishna Rajak\*

Three complexes  $[Zn_2(L)_2(\mu^{1,2}\text{-OAc})(\mu^{1,1}\text{-OAc})] \cdot C_9H_8N_2$  **1**,  $[Zn_3(L)_4] \cdot (ClO_4)_2$  **2** and  $[Zn(L)_2] \cdot CH_3OH$  **3** were synthesized using a common Schiff base 2,4-dimethyl-6-((quinolin-8-ylimino)methyl)phenol (HL) and characterized by various methods such as elemental analysis,  $^1H$  NMR, FT-IR, UV-Vis and mass spectroscopy. The single crystal XRD analysis revealed that complex **1** is dinuclear, complex **2** trinuclear and complex **3** mononuclear in nature. The photophysical properties of the ligand and complexes were also investigated by different techniques such as UV-Vis spectroscopy, fluorescence spectroscopy, fluorescence lifetime measurement, DFT, and TDDFT calculations in solvents of different polarity. The complexes exhibited higher quantum yields than the ligand in solution. The trinuclear complex had higher emission intensity than the mono and dinuclear complexes in solution as well as in the solid state. In addition, complex **1** exhibited a unique dissymmetric coordination mode of the oxygen atom in the acetate bridging moiety.

Received 1st November 2014  
Accepted 28th November 2014

DOI: 10.1039/c4ra13606c

www.rsc.org/advances

### Introduction

Schiff bases play a vital role in modern coordination chemistry,<sup>1–3</sup> where tridentate salen-type ligands are one of the most popular classes<sup>4–6</sup> of Schiff-base ligands amongst the coordination chemists. These systems possess an extra dimension to their optical properties as metal coordination significantly alters the photophysical processes they are capable of. These intriguing metal coordination-driven photophysical properties have enabled various applications including the development of nonlinear optical materials,<sup>7–9</sup> sensitizers for solar cells,<sup>10,11</sup> and metal ion sensors.<sup>12–14</sup>

Salen type complexes have an important aspect of their emission behavior. In most cases, metal coordination enhances the charge-transfer character in the excited state of the chromophores. The fluorescence of the salen type complexes<sup>15–17</sup> with several elements is very strong, particularly the salen type-zinc(II) complexes which exhibit electroluminescence as well as photoluminescence.<sup>18,19</sup> The organic fluorescent materials have attracted intensive interest because of their potential applications in organic light emitting diodes (OLED), organic field effect transistors (OFET), fluorescent sensors, *etc.*<sup>20</sup> Conventional fluorescent dyes of large delocalized  $\pi$ -conjugated moieties typically suffer from fluorescence quenching at high

concentrations or in aggregated states, and thus cannot serve as ideal fluorescent compounds.

A diversity of fluorescent-sensing approaches have been extensively investigated pertaining to the signaling mechanisms of metal–ligand charge transfer (MLCT),<sup>21a</sup> internal charge transfer (ICT),<sup>21b</sup> photo induced electron transfer/energy transfer (PET),<sup>21c</sup> metal–ligand charge transfer (MLCT),<sup>21d</sup> excimer/excimer formation as well as the excited state intramolecular/intermolecular proton transfer (ESIPT).<sup>21d</sup> The fluorescence of the ligand (HL) appears due to ESIPT<sup>6</sup> mechanism but the emission intensity is very weak in contrast with the complexes, probably due to quenching by the lone pair of electrons of the donor atoms in the ligands through the PET mechanism.<sup>21c</sup> For Zn(II) complexes, no emission originating from metal-centered MLCT/LMCT excited states are expected, since the Zn(II) ion is difficult to be oxidized or reduced due to its stable  $d^{10}$  configuration. Thus, the emission observed in the complexes is tentatively assigned to the  $\pi \rightarrow \pi^*$  intraligand fluorescence.<sup>22</sup> Moreover, in complex the PET<sup>21c</sup> process is prevented by the complexation of HL with metal ions, as well as CHEF<sup>23,24</sup> mechanism which reduces the loss of energy by thermal vibrational decay<sup>21</sup> enhances emission intensity during complexation. The lattice structure of dinuclear complex contains non coordinated free amine in solid state and it undergoes PET process to quench its emission intensity.

Our strategy is to change the concentration ratio of metal and ligand and then synthesize different types of polynuclear complexes to find the genesis behind their different photophysical phenomena. Recently, we reported the synthesis and the structure of a Zn(II)-mononuclear complex  $[ZnL_2]$ .<sup>6</sup> This bischelate Zn(II) complex displayed a moderately strong

*Inorganic Chemistry Section, Department of Chemistry, Jadavpur University, Kolkata, 700 032, India. E-mail: kajalrajak@hotmail.com*

† Electronic supplementary information (ESI) available: X-ray crystallographic file in CIF format for **1** and **2**; Fig. S1–S17 and Tables S1–S5. CCDC 1015063 and 1015064. For ESI and crystallographic data in CIF or other electronic format see DOI: 10.1039/c4ra13606c

fluorescence in THF solution. We synthesized **HL** in different ways besides the two unique coordination modes of dinuclear and trinuclear Zn(II) complexes, synthesized to achieve our goal. Our main focus was to compare the change in excited state emission behavior of the above stated complexes in solution state and in solid state. Interestingly, the complexes show significant differences but maintain a regular trade in their photoluminescence behaviors.

Here we report an unexpected and exclusive formation of bisacetato bridged dinuclear complex, which contain different mode of coordination with the oxygen atom of acetate group. We also focus on how different modes of coordination of acetate group can modulate the geometrical environment of central atom from trigonal bipyramide to square pyramidal shape.

Some aspects of these unforeseen findings were rationalized by DFT and TDDFT calculations. We also calculated and analyzed the singlet ground state natural transition orbitals (NTOs) derived from TDDFT results and compared them with the ground state molecular orbitals (MOs) obtained from DFT calculations. The computational modeling of the NMR parameter is also of abiding interest, and such DFT calculations have emerged as a promising approach for the prediction of nuclear shielding and coupling constants of NMR active nuclei.<sup>25</sup> Thus, we computed the proton NMR chemical shifts and also the <sup>1</sup>H–<sup>1</sup>H spin–spin coupling constant using the gauge-independent atomic orbital (GIAO)-DFT method, which was aimed at providing the definitive characterization of the complexes. The solid-state structure of the complexes stays in solution, as revealed by the combined experimental and theoretical NMR spectral analyses.

## Experimental section

### Materials

3,5-Dimethyl phenol was purchased from sigma Aldrich. Zn(OAc)<sub>2</sub>·2H<sub>2</sub>O. All the solvents were spectroscopic grade and used after proper distillation. The purity was also verified by recording the emission spectra in the studied spectral region. Zinc perchlorate hexahydrate was prepared by the standard procedure.

**Caution!** Perchlorate salts are potentially explosive and should be handled with care and in small amounts, although we encountered no problems.

### Physical measurements

UV-Vis spectra were recorded on a Perkin-Elmer LAMBDA 25 spectrophotometer. IR spectra were recorded on a Perkin-Elmer L-0100 spectrophotometer. <sup>1</sup>H NMR spectra were measured on Bruker FT 300 MHz spectrometer with TMS as the internal standard. Elemental analyses (C, H, N) were performed on Perkin-Elmer 2400 series II analyzer. The molar conductivity was determined using Systronics Conductivity Meter 304 in acetonitrile solution at room temperature. Electrospray ionization mass spectrometry (ESI-MS) measurements were done on a Micromass Qtof YA 263 mass spectrometer using acetonitrile as a solvent. The emission data were collected on a Perkin-Elmer

LS 55 fluorescence spectrometer. For the luminescence measurements, excitation and emission slit width of 5 nm was used for the complex and 10 nm slit width for the ligand. Quantum yields of the complexes were determined in freeze-pump-thaw-degassed solutions of the complexes by a relative method using quinine sulfate in the same solvent as the standard [ $\Phi_{\text{std}} = 0.54$  (at 298 K) in 0.1 M H<sub>2</sub>SO<sub>4</sub> at  $\lambda_{\text{ex}} = 350$  nm]<sup>26b</sup> by usual method. The fluorescence life time was determined by usual method.<sup>26a</sup>

### Computational details

The geometrical structures of the singlet ground state (S<sub>0</sub>) were optimized in solution by the DFT<sup>27</sup> method with B3LYP exchange correlation functional<sup>28</sup> approach. The vibrational frequency calculation was also performed for the complexes to ensure that the optimized geometries represent the local minima and there are only positive eigen values. On the basis of these optimized ground state geometry structure, the absorption spectral properties in solvents with different polarity were calculated by TDDFT<sup>29</sup> associated with the conductor-like polarizable continuum model (CPCM).<sup>30</sup> TDDFT calculations were performed for complex **1** only as both the complexes show similar nature. We computed the lowest 40 singlet–singlet transition.

The effective core potential (ECP) approximation of Hay and Wadt was used for describing the (1s<sup>2</sup>2s<sup>2</sup>2p<sup>6</sup>) core electron for zinc whereas the associated “double- $\xi$ ” quality basis set LANL2DZ was used for the valence shell.<sup>31,32</sup> 6-311+G and 6-311+G\* basis sets were used for H atom and for C, N and O atoms respectively. The calculated electronic density plots for frontier molecular orbitals were prepared by using the Gauss View 5.0 software. All the calculations were performed with the Gaussian 09W software package.<sup>33</sup> Gauss Sum 2.1 program<sup>34</sup> was used to calculate the molecular orbital contributions from groups or atoms.

In addition, the <sup>1</sup>H NMR properties of the complexes were calculated with the magnetic field perturbation method with the GIAO algorithm<sup>35</sup> with the NMR = spin–spin keyword incorporated in the Gaussian 09W program. In calculation, the 6-311+G (2d,p) basis set was employed for non-metal. The relative chemical shift of a given nucleus X in the molecule was defined as  $\delta_{\text{X}}^{\text{calc}}$  [ppm] =  $\sigma_{\text{X}}^{\text{ref}} - \sigma_{\text{X}}^{\text{calc}}$  where TMS was used as a reference molecule optimized at the same level of theory.<sup>35b,36a</sup> In order to account for the solvent effect, we used the integral equation-formalism polarizable continuum model (IEFPCM) method.<sup>36b,c</sup>

### Crystallographic studies

The X-ray intensity data of single crystals of compound **1** and **2** were collected on Bruker AXS SMART APEX CCD diffractometer (Mo K $\alpha$ ,  $\lambda = 0.71073$  Å) at 293 K. The data were reduced in SAINTPLUS<sup>37</sup> and empirical absorption correction was applied using the SADABS package.<sup>37</sup> Metal atom was located by Patterson Method and the rest of the non-hydrogen atoms were generated from successive Fourier synthesis. The structures were refined by full matrix least-square procedure on  $F^2$ . All non-hydrogen atoms were refined anisotropically. Calculations

were performed using the SHELXTL V 6.14 program package.<sup>38</sup> For complex 2, a solvent void remained in which no satisfactory solvent model could be constructed and thus the structure was refined using the SQUEEZE option of PLATON program. The squeeze output was also appended in the CIF file of complex 2. Molecular graphics were drawn using ORTEP<sup>39a</sup> and Mercury<sup>39b</sup> softwares. The relevant crystal data are given in Table 1.

### Synthesis of 2-hydroxy-3,5-dimethylbenzaldehyde (A)

A mixture of 3.5 g (25 mmol) of 2,4-dimethylphenol, 1.89 g (13.5 mmol) of hexamethylenetetramine and 1.89 g (21 mmol) of paraformaldehyde was heated to 100 °C, with stirring. 7.5 mL of acetic acid was then added drop wise. The whole system was brought to 110 °C. over a period of 15 minutes, with stirring. 1.7 mL of sulphuric acid and 0.6 mL of water were then added drop wise over a period of 15 minutes. Stirring was continued at 110 °C. for 30 minutes, and then the mixture was poured into 50 mL of hot water. The preparation was extracted 3 times with methylene chloride, and then the combined organic phases were washed until neutral with an aqueous sodium hydrogen carbonate solution. Drying over sodium sulphate, evaporation and removal of the solvent by distillation yielded 3.04 g (80%) of yellow oil. Elemental anal. calc. for C<sub>9</sub>H<sub>10</sub>O<sub>2</sub>: C, 71.98; H, 6.71. Found: C, 72.09; H, 6.68%. <sup>1</sup>H NMR {300 MHz, CDCl<sub>3</sub>, δ (ppm), J (Hz)}: 11.07 (CHO, s), 9.80 (OH, s), 7.25–7.15 (2H, ArH), 2.29, (CH<sub>3</sub>, s), 2.18 (CH<sub>3</sub>, s). ESI-MS (CH<sub>3</sub>CN): *m/z* calc. 150.0681, found: 151.0772 (100%) (A + H)<sup>+</sup>.

**Preparation of ligand [2,4-dimethyl-6-((quinolin-8-ylimino)-methyl)phenol] (HL).** 3 g (20 mmol) of 2-hydroxy-3,5-dimethylbenzaldehyde (A) and 2.88 g (20 mmol) of 8-aminoquinoline were taken in 50 mL methanol solution. Then the mixture was refluxed in water bath for 2 hours. The solvent was removed under reduced pressure to obtain the desired ligand (HL).

Yield 4.6 g (83%). Elemental anal. calc. for C<sub>18</sub>H<sub>16</sub>N<sub>2</sub>O: C, 78.24; H, 5.84; N, 10.14. Found: C, 78.85; H, 5.69; N, 10.22%. <sup>1</sup>H NMR {300 MHz, CDCl<sub>3</sub>, δ (ppm), J (Hz)}: 8.16 (CH=N, s), 4.98 (OH, bs) 7.69–7.16 (8H, ArH), 2.33 (CH<sub>3</sub>, s), 2.30 (CH<sub>3</sub>, s). Selected FT-IR bands (KBr, cm<sup>-1</sup>): 3543 (b), 3454 (s), 3348 (s), 3033 (w), 1962 (w), 1616 (s), 1565 (m), 1498 (s), 1467 (s), 1363 (s), 1332 (s), 1270 (w), 1130 (m), 1080 (m), 793 (s). ESI-MS (CH<sub>3</sub>CN): *m/z* calc. 277.1341, found: 277.1502 (100%) (HL + H)<sup>+</sup>, 300.2122 (52%) (HL + Na)<sup>+</sup>.

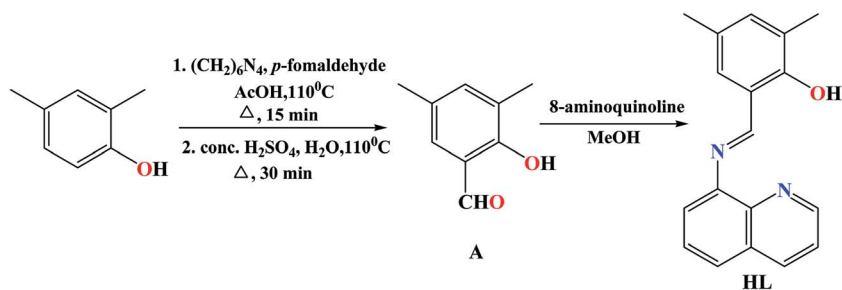
### Synthesis of complexes

**[Zn<sub>2</sub>(L)<sub>2</sub>(μ<sup>1,2</sup>-OAc)(μ<sup>1,1</sup>-OAc)]·C<sub>9</sub>H<sub>8</sub>N<sub>2</sub>, 1·C<sub>9</sub>H<sub>8</sub>N<sub>2</sub>.** To the CH<sub>3</sub>CN solution (20 mL) of HL (0.276 g, 1.00 mmol), methanolic solution (10 mL) of Zn(OAc)<sub>2</sub>·2H<sub>2</sub>O (0.219 g, 1.00 mmol) was added drop wise followed by NEt<sub>3</sub> (140 mL, 0.102 g, 2.00 mmol) and stirred for 4 h at room temperature. The color of the solution was changed from colorless to intense orange. The solution was kept for slow evaporation. The orange single crystals suitable for single-crystal X-ray analysis were obtained from CH<sub>3</sub>CN solution after one week. Yield: 375 mg (80%). Elemental anal. calc. for C<sub>49</sub>H<sub>44</sub>N<sub>6</sub>O<sub>6</sub>Zn<sub>2</sub>: C, 62.36; H, 4.70; N, 8.91. Found: C, 62.48; H, 4.61; N, 8.88%. <sup>1</sup>H NMR<sub>expt</sub> {300 MHz, CDCl<sub>3</sub>, δ (ppm), J (Hz)}: 8.74 (H10, s), 8.34 (H1, d, J = 4.8), 7.77–6.88 (8H, ArH), 2.40 (H17, s), 2.02 (H40, s). <sup>1</sup>H NMR<sub>theor</sub> {δ (ppm) aq = aminoquinoline, Me = methyl, ace = acetate and al = aldehyde }: 8.68 (H10), 8.54 (H1), 7.93 (H3), 7.66 (H2), 7.47 (H7), 7.30 (H5), 7.10 (H14), 6.58 (H12), 2.31 (H35, CH<sub>3</sub>[ace]) and 1.93 (H38, CH<sub>3</sub>[al]). Selected FT-IR<sub>expt</sub> bands (KBr, cm<sup>-1</sup>): 3452 (b), 2918 (w), 2358 (s), 2330 (s), 1561 (s), 1363 (s), 1219 (s), 1046 (m), 825(m). IR<sub>theor</sub> (ν cm<sup>-1</sup>): (<sup>aq</sup>C–H<sub>asym</sub>) 3218, 3220, 3229 and 3236 (<sup>aq</sup>C–H<sub>sym</sub>) 3193, 3196, 3204, 3206 and 3209; (<sup>Me</sup>C–H<sub>sym</sub>) 3005 and 2987; (C=N<sub>sym</sub>) (<sup>ace</sup>C=O<sub>asym</sub>) 1605, 1601; (<sup>Me</sup>C–H<sub>vib</sub>) 1537 and 1541; ν(<sup>al</sup>C–H<sub>vib</sub>) 1360 (<sup>al</sup>C–O<sub>sym</sub>) 1365 and (<sup>ace</sup>C–O<sub>sym</sub>) 1363.

Table 1 Crystal data and structure refinement parameters for complex 1·C<sub>9</sub>H<sub>8</sub>N<sub>2</sub> and 2

	[Zn <sub>2</sub> (L) <sub>2</sub> (μ <sup>1,2</sup> -OAc)(μ <sup>1,1</sup> -OAc)]·C <sub>9</sub> H <sub>8</sub> N <sub>2</sub> , 1·C <sub>9</sub> H <sub>8</sub> N <sub>2</sub>	[Zn <sub>3</sub> (L) <sub>4</sub> ](ClO <sub>4</sub> ) <sub>2</sub> , 2
Formula	C <sub>49</sub> H <sub>44</sub> N <sub>6</sub> O <sub>6</sub> Zn <sub>2</sub>	C <sub>72</sub> H <sub>58</sub> Cl <sub>2</sub> N <sub>8</sub> O <sub>12</sub> Zn <sub>3</sub>
<i>M<sub>r</sub></i>	943.68	1494.33
Crystal system	Triclinic	Monoclinic
Space group	<i>P</i> 1	<i>C</i> 2/ <i>c</i>
<i>a</i> /Å	8.262(2)	24.966(9)
<i>b</i> /Å	14.563(3)	20.629(7)
<i>c</i> /Å	18.991(4)	16.929(6)
α/°	75.372(10)	90
β/°	77.580(10)	111.647(2)
γ/°	84.010(10)	90
<i>V</i> /Å <sup>3</sup>	2156.53(8)	8104.1(5)
<i>Z</i>	2	4
<i>D</i> <sub>calcd</sub> /mg m <sup>-3</sup>	1.453	1.225
μ/mm <sup>-1</sup>	1.171	1.004
θ/°	1.1–27.5	1.8–27.6
<i>T</i> /K	293(2)	293(2)
Reflns collected	9814	9438
<i>R</i> <sub>1</sub> , <sup>a</sup> <i>wR</i> <sub>2</sub> <sup>b</sup> [ <i>I</i> > 2σ( <i>I</i> )]	0.044, 0.137	0.062, 0.182
GOF on <i>F</i> <sup>2</sup>	1.07	1.01

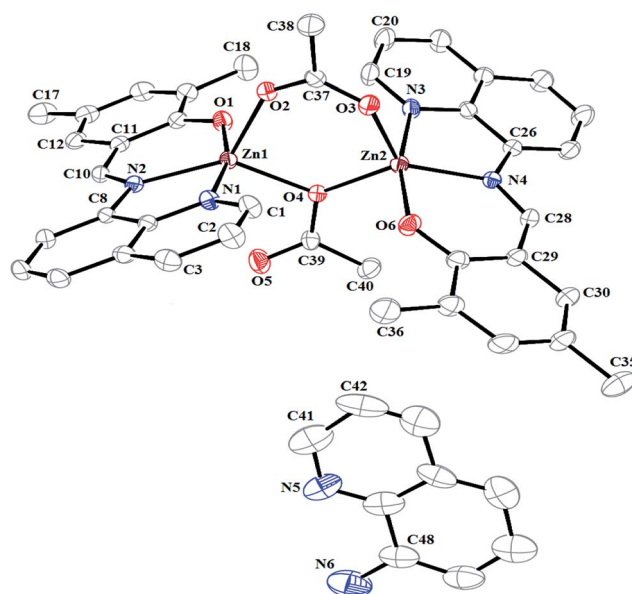
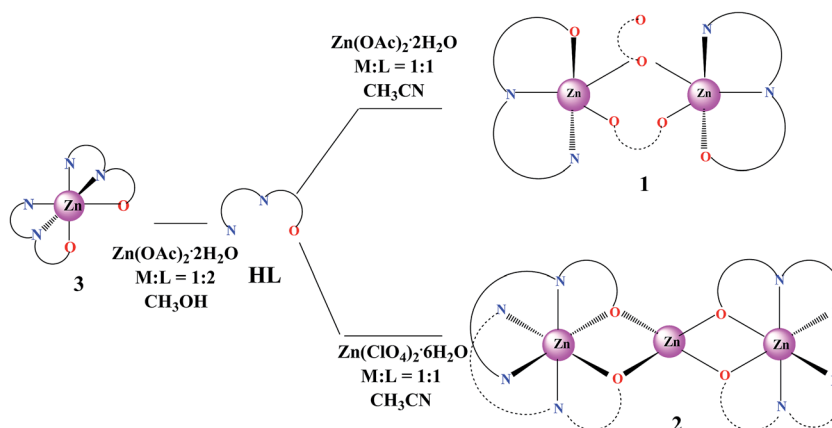
$$^a R_1 = \sum |F_o| - |F_c| / \sum |F_o|. \quad ^b wR_2 = [\sum [w(F_o^2 - F_c^2)^2] / \sum [w(F_o^2)^2]]^{1/2}.$$



Scheme 1 Schematic representation for the synthesis of the ligand.

ESI-MS ( $\text{CH}_3\text{CN}$ ):  $m/z$  calcd 740.4173, found: 740.3229 (100%). Molar conductance,  $\Lambda_M$ : ( $\text{CH}_3\text{CN}$  solution)  $8 \Omega^{-1} \text{cm}^2 \text{mol}^{-1}$ .

$[\text{Zn}_3(\text{L})_4] \cdot (\text{ClO}_4)_2 \cdot 2$ . To the  $\text{CH}_3\text{CN}$  solution (20 mL) of HL (0.276 g, 1.00 mmol), methanolic solution (10 mL) of  $\text{Zn}(\text{ClO}_4)_2 \cdot 6\text{H}_2\text{O}$  (0.372 g, 1.00 mmol) was added dropwise followed by  $\text{NEt}_3$  (140 mL, 0.102 g, 2.00 mmol). The reaction mixture was refluxed under water bath for 2 h, then cooled and stirred for 6 h at RT. The color of the solution changed from colorless to intense orange. The solution was kept for slow evaporation. The orange single crystals suitable for single-crystal X-ray analysis were obtained from solution after 2 days. Yield: 4.25 g (84%). Elemental anal. calc. for  $\text{C}_{72}\text{H}_{58}\text{Cl}_2\text{N}_8\text{O}_{12}\text{Zn}_3$ : C, 57.87; H, 3.91; N, 7.50. Found: C, 57.95; H, 3.87; N, 7.57%.  $^1\text{H NMR}$  {300 MHz,  $\text{CDCl}_3$ , d (ppm),  $J$  (Hz)}: 8.804 (H1, s), 8.75 (H10, d,  $J = 5.9$ ), 8.09–7.76 (8H, ArH), 2.18 (H27, s), 2.14 (H26, s).  $^1\text{H NMR}_{\text{theor}}$   $\{\delta$  (ppm)}: 8.77 (H1), 8.68 (H10), 8.07 (H3), 7.86 (H2), 7.71 (H7), 7.59 (H5), 7.74 (H14), 7.52 (H12), 2.11 (H17,  $-\text{CH}_3[\text{al}]$ ) and 2.19 (H18,  $-\text{CH}_3[\text{al}]$ ). Selected FT-IR bands (KBr,  $\text{cm}^{-1}$ ): 3488 (b), 2918 (w), 2361 (s), 1843 (s), 1770 (s), 1653 (s), 1418 (s), 1269 (m), 1219(b), 1048 (w), 810 (w).  $\text{IR}_{\text{theor}}$  ( $\nu \text{cm}^{-1}$ ): ( $^{13}\text{C}-\text{H}_{\text{asym}}$ ) 3324, 3308, 3289 and 3265; ( $^{13}\text{C}-\text{H}_{\text{sym}}$ ) 3213, 3209, 3195 and 3190; ( $^{13}\text{C}-\text{H}_{\text{sym}}$ ) 3017 and 3001; ( $^{13}\text{C}=\text{NH}_{\text{sym}}$ ) 1614; ( $^{13}\text{C}-\text{H}_{\text{vib}}$ ) 1542 and 1536; ( $^{13}\text{C}-\text{H}_{\text{vib}}$ ) 1524 and 1518; ( $^{13}\text{C}-\text{H}_{\text{vib}}$ ) 1362 and ( $^{13}\text{C}-\text{O}_{\text{sym}}$ ) 1365. ESI-MS ( $\text{CH}_3\text{CN}$ ):  $m/z$  calcd 646.8229, found: 646.9227 (100%). Molar conductance,  $\Lambda_M$ : ( $\text{CH}_3\text{CN}$  solution)  $252 \Omega^{-1} \text{cm}^2 \text{mol}^{-1}$ .

Fig. 1 Asymmetric unit of complex 1· $\text{C}_9\text{H}_8\text{N}_2$  with displacement ellipsoids drawn at the 25% probability level. Hydrogen atoms have been omitted for clarity.

Scheme 2 Schematic representation for the synthesis of the complexes.

Table 2 Selected bond distance (Å) for complex 1 and 2

Bond length			
[Zn <sub>2</sub> (L) <sub>2</sub> (μ <sup>1,2</sup> -OAc)(μ <sup>1,1</sup> -OAc)]·C <sub>9</sub> H <sub>8</sub> N <sub>2</sub> , 1		[Zn <sub>3</sub> (L) <sub>4</sub> ](ClO <sub>4</sub> ) <sub>2</sub> , 2	
Zn1–O1	1.988(2)	Zn2–O3	2.000(3)
Zn1–O2	2.098(2)	Zn2–O4	2.029(18)
Zn1–O4	2.066(19)	Zn2–O6	1.999(2)
Zn1–N1	2.148(3)	Zn2–N3	2.166(3)
Zn1–N2	2.077(2)	Zn2–N4	2.086(2)
Zn1–O1	2.133(3)	Zn1–N4	2.150(3)
Zn1–O2	2.140(3)	Zn2–O1	1.954(3)
Zn1–N1	2.150(3)	Zn2–O2	1.940(3)
Zn1–N2	2.095(3)	Zn2–O1 <sup>i</sup>	1.954(3)
Zn1–N3	2.122(3)	Zn2–O2 <sup>i</sup>	1.940(3)

## Result and discussion

### Synthesis of the probe

The preparation of Schiff base 2,4-dimethyl-6-((quinolin-8-ylimino)methyl)phenol (**HL**) was presented in Scheme 1. The stoichiometric reaction of Zn(OAc)<sub>2</sub>·2H<sub>2</sub>O with the ligand **HL** in acetonitrile produced the orange colored acetate bridge dinuclear complex 1·C<sub>9</sub>H<sub>8</sub>N<sub>2</sub> in good yields. However, when the same reaction was carried out in presence of stoichiometric amounts of Zn(ClO<sub>4</sub>)<sub>2</sub>·6H<sub>2</sub>O it gave a dark orange colored phenoxo bridge trinuclear complex, 2. In these complexes, the ligand **HL** bound as a monoanionic N, N, O coordinating tridentate ligand and formed neutral complex 1·C<sub>9</sub>H<sub>8</sub>N<sub>2</sub>, whereas complex 2 showed cationic nature. The molar conductivity values of both the complexes were determined in acetonitrile solution at room temperature. The values of the molar conductivity were 8 and 252 Ω<sup>-1</sup> cm<sup>2</sup> mol<sup>-1</sup> for 1·C<sub>9</sub>H<sub>8</sub>N<sub>2</sub> and 2, respectively. The value for complex 2 corresponded to a 2 : 1 type of electrolyte behavior,<sup>40</sup> whereas the complex 1·C<sub>9</sub>H<sub>8</sub>N<sub>2</sub> was nonconductance.

A schematic representation for the synthesis of complexes is given in Scheme 2. The elemental analysis and Electrospray ionization mass spectroscopic measurements confirmed the formation of the synthesized complexes (see Experimental section).

### Crystal structures

[Zn<sub>2</sub>(L)<sub>2</sub>(μ<sup>1,2</sup>-OAc)(μ<sup>1,1</sup>-OAc)]·C<sub>9</sub>H<sub>8</sub>N<sub>2</sub>, 1·C<sub>9</sub>H<sub>8</sub>N<sub>2</sub>. The asymmetric units of complex 1 contain two L<sup>-</sup>, two Zn(II) ion, two acetate anion and one free amine (Fig. 1). The geometry around the Zn1 atom is intermediate between square based pyramid and distorted trigonal bipyramid (τ = 0.48) whereas that of Zn2 is distorted trigonal bipyramidal (τ = 0.63).<sup>41</sup> The equatorial positions at Zn1 are occupied by O2, N2 and O4 atoms and the axial position are engaged by N1 and O1 respectively, while for Zn2 center the equatorial positions are occupied by O3, O4 and N4 atoms and axial positions are engaged by O6 and N3 respectively. The Zn(II) ions in complex 1 have the same coordination environment as that of ZnN<sub>2</sub>O<sub>3</sub> in which the Zn–O and Zn–N bond distances vary between 1.988(2)–2.098(2) Å and

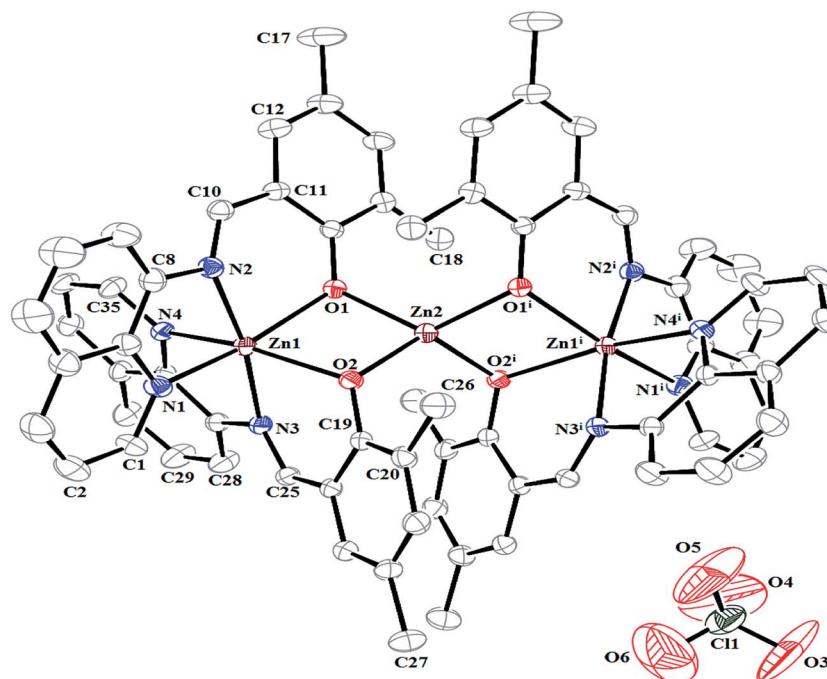


Fig. 2 Asymmetric unit of complex 2, with displacement ellipsoids drawn at the 30% probability level. Hydrogen atoms have been omitted for clarity.

Table 3 Selected bond angle ( $^{\circ}$ ) for complex 1 and 2<sup>a</sup>

Bond angle ( $^{\circ}$ )							
[Zn <sub>2</sub> (L) <sub>2</sub> (μ <sup>1,2</sup> -OAc)(μ <sup>1,1</sup> -OAc)]·C <sub>9</sub> H <sub>8</sub> N <sub>2</sub> , 1		[Zn <sub>3</sub> (L) <sub>4</sub> ]·(ClO <sub>4</sub> ) <sub>2</sub> , 2					
O1–Zn1–O2	92.53(9)	O3–Zn2–O4	103.40(8)	O1–Zn1–O2	77.05(10)	N1–Zn1–N3	96.37(12)
O1–Zn1–O4	98.03(8)	O3–Zn2–O6	96.81(10)	O1–Zn1–N1	160.33(11)	N1–Zn1–N4	95.58(13)
O1–Zn1–N1	165.85(9)	O3–Zn2–N3	93.16(11)	O1–Zn1–N2	85.09(11)	N2–Zn1–N3	171.89(14)
O1–Zn1–N2	89.58(9)	O3–Zn2–N4	128.34(9)	O1–Zn1–N3	101.14(11)	N2–Zn1–N4	96.00(12)
O2–Zn1–O4	92.35(8)	O4–Zn2–O6	94.86(9)	O1–Zn1–N4	96.69(11)	N3–Zn1–N4	78.24(12)
O2–Zn1–N1	90.45(9)	O4–Zn2–N3	92.57(9)	O2–Zn1–N1	96.52(12)	O1–Zn2–O2	86.25(11)
O2–Zn1–N2	129.90(9)	O4–Zn2–N4	127.30(9)	O2–Zn1–N2	103.91(11)	O1–Zn2–O1 <sup>i</sup>	119.59(11)
O4–Zn1–N1	95.67(9)	O6–Zn2–N3	165.84(10)	O2–Zn1–N3	82.70(11)	O1–Zn2–O2 <sup>i</sup>	126.28(10)
O4–Zn1–N2	136.82(9)	O6–Zn2–N4	88.92(9)	O2–Zn1–N4	158.41(11)	O1 <sup>i</sup> –Zn2–O2	126.28(10)
N1–Zn1–N2	77.94(9)	N3–Zn2–N4	76.99(10)	N1–Zn1–N2	78.38(13)	O2–Zn2–O2 <sup>i</sup>	116.93(11)
				O1 <sup>i</sup> –Zn2–O2 <sup>i</sup>	86.25(11)	Zn1–O2–Zn2	97.42(11)
				Zn1–O1–Zn2	97.63(10)		

<sup>a</sup> <sup>i</sup>Symmetry code:  $-x, y, 1/2 - z$ .

2.077(2)–2.166(3) Å, respectively (Table 2). The ligand acts as a mono anionic tridentate chelated ligand with *N, N, O* donors in each metal centre. The two acetate groups bridged the Zn1 and

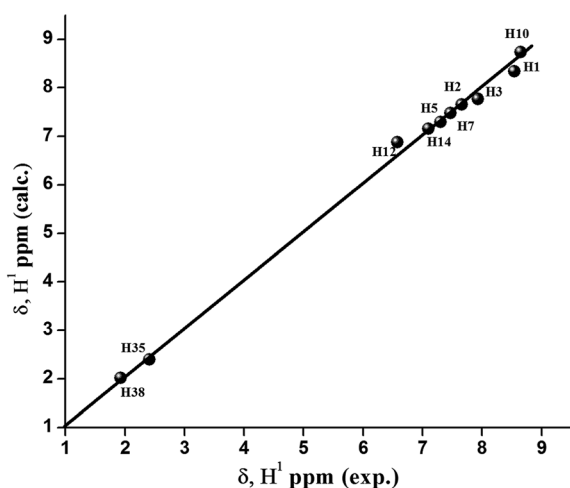


Fig. 3 Linear correlation between the experimental and calculated <sup>1</sup>H NMR chemical shifts of 1 in aliphatic and aromatic regions.

Zn2 ions by two different bridging fashions syn–syn μ<sup>1,2</sup> bidentate and μ<sup>1,1</sup> monodentate resulting in diacetato bridged dinuclear Zn(II) complex.

[Zn<sub>3</sub>(L)<sub>4</sub>]·(ClO<sub>4</sub>)<sub>2</sub>, 2. The crystal structure of complex 2 consists of discrete tri nuclear [Zn<sub>3</sub>(L)<sub>4</sub>]<sup>2+</sup> cation and two isolated perchlorate anions in the ratio of 1 : 2. The asymmetric units of complex 2 contain two Zn(II) ions, two L<sup>−</sup> and two ClO<sub>4</sub> anion (Fig. 2). Two different types of coordination environment are observed around the Zn(II) ions. The terminal zinc atoms Zn1 and Zn1<sup>i</sup> are symmetrically equivalent and hexacoordinated. The bond lengths and angles are given in the Tables 2 and 3. The central Zinc atom Zn2 adopts tetrahedral coordination environment with four oxygen donor atoms. The distance between Zn1–Zn2 is 3.074 Å. The bond lengths of Zn–N and Zn–O in Zn1 vary in the range 2.129 and 2.136 respectively. The bond lengths of Zn–O in Zn2 vary in the range 1.947. In complex 2, angular Zn1–Zn2–Zn1<sup>i</sup> disposition is nearly 170°. The Zn1 is distorted in octahedral geometry which is coordinated by two phenoxido oxygen atoms (O1 and O2), two pyridyl nitrogen of the quinoline moiety (N1 and N4) and two imine nitrogen atoms (N2 and N3) of the ligands. In octahedral geometry, *cis* angles ranging from 77 to 103 and the *trans* angle

Table 4 Frontier molecular orbital composition (%) in the ground state for 1

Orbital	Energy (eV)	Contribution (%)				Main bond type
		Zn (M)	Acetate (OAc)	Quinoline (Qu)	Aldehyde (al)	
L + 4	−0.98	0	0	99	1	π* (Qu)
L + 3	−1.31	0	0	56	43	π* (Qu) + π* (al)
L + 2	−1.56	0	0	61	38	π* (Qu) + π* (al)
L + 1	−2.13	0	0	73	27	π* (Qu) + π* (al)
LUMO	−2.37	0	0	68	32	π* (Qu) + π* (al)
HOMO	−5	0	1	15	83	π (Qu) + π (al)
H − 1	−5.3	1	1	15	83	π (Qu) + π (al)
H − 2	−6.01	1	1	46	51	π (Qu) + π (al)
H − 3	−6.19	7	5	24	64	M(d) + π (OAc) + π (Qu) + π (al)
H − 4	−6.28	6	3	40	51	M(d) + (OAc) + π (Qu) + π (al)
H − 5	−6.43	7	35	16	42	M(d) + (OAc) + π (Qu) + π (al)

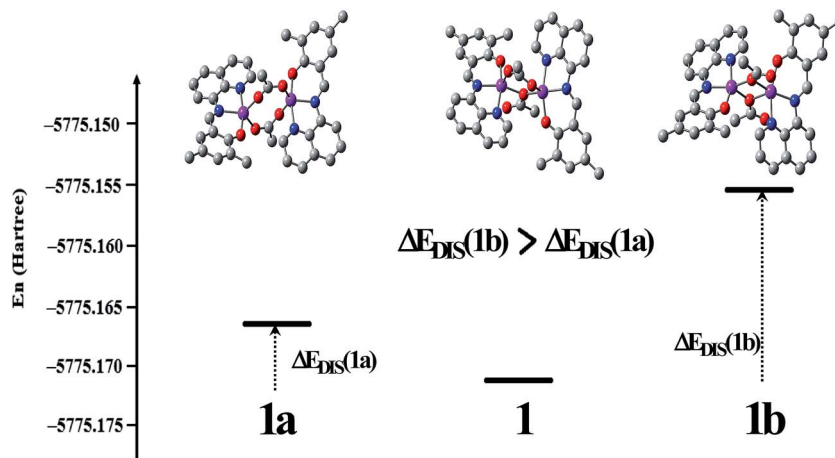


Fig. 4 Optimized energy diagram with optimized molecular structures of **1**, **1a** and **1b**. (Zn: pale violet, N: blue, O: red, C: grey. Hydrogen atoms are omitted for clarity)  $\Delta E_{\text{DIS}}$  means the destabilization energy gap.

from 158 to 178° clearly indicates the amount of distortion. In contrast, Zn2 is tetrahedral coordinated by four phenoxo oxygen atom from the four individual ligands.

### Mass spectra

The ligand (**HL**) and the desired aldehyde (**A**) were diluted with acetonitrile for mass spectrometry. Mass spectral analysis in the positive ion mode showed a major peak at  $m/z$  (%) = 277.1502 (100), 300.2122 (60) and 151.0772 (100), which were assigned to the mono cationic form of  $[\text{HL} + \text{H}]^+$ ,  $[\text{HL} + \text{Na}]^+$  and  $[\text{A} + \text{H}]^+$  respectively. The mass spectrum of the **HL** and **A** are given in ESI Fig. S1 and S2.† The mass spectra of complexes **1** and **2** were carried out in acetonitrile solution. A major peak appeared at  $m/z$  (%) = 740.3229 (100) and 646.9227 (100), which was allocated for the mono-cationic monoacetate bridging of dinuclear complex  $[\text{Zn}_2(\text{L})_2(\mu\text{-OAc})]^+$  and bicationic trinuclear complex  $[\text{Zn}_3(\text{L})_4]^{2+}$  respectively. The mass spectrums of the complexes are given in ESI Fig. S3 and S4.† It also suggested that in solutions the major species existing are as same as the molecular formula in their solid state.

### NMR spectra

The ligand (**HL**), the desired aldehyde (**A**) and complexes are diamagnetic and display well resolved  $^1\text{H}$  NMR spectra. For complex **1**, (**A**) and **HL**,  $^1\text{H}$  NMR spectra were done in  $\text{CD}_3\text{Cl}$  solution, whereas, complex **2** was dissolved in  $\text{CD}_3\text{CN}$  solution respectively. A sharp singlet peak of aldehyde proton of (**A**) was

Table 6 Photophysical parameters of the ligands in different solvent at room temperature

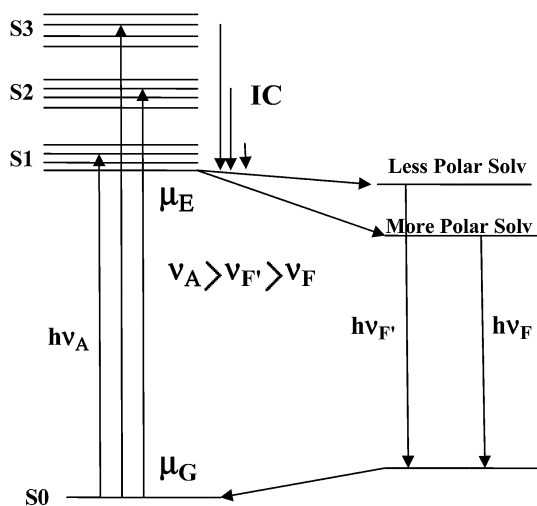
Solvent	$\lambda_{\text{abs}}$	$\lambda_{\text{em}}$	$(\Phi_{\text{f}})^a$	$\tau$ (ns)	$\chi^2$	$k_{\text{r}} \times 10^7$	$k_{\text{nr}} \times 10^9$
Hexane	323	419	2.98	0.91	1.13	3.2	1.06
$\text{CCl}_4$	325	445	2.86	0.94	1.21	3.0	1.06
DCM	329	457	2.67	1.01	0.91	2.6	0.96
Acetone	332	464	1.02	1.53	0.89	0.67	0.64
$\text{CH}_3\text{CN}$	342	476	0.78	2.27	1.01	0.42	0.51
DMF	348	480	0.73	3.01	1.19	0.32	0.44

$a = 10^{-2}$ .

observed at strongly deshielding field near at 11.07 ppm and the peak appeared at 9.80 ppm mainly responsible for phenolic proton. Two doublet aromatic protons appeared at aromatic span 7.25–7.15 ppm. Two sharp singlet peaks appeared at a higher shielding field near 2.29 and 2.18 ppm due to the two methyl proton in ESI Fig. S5.† The peak that appeared at high deshielding field for aldehyde proton in (**A**) completely disappeared in  $^1\text{H}$  NMR spectra of **HL**, whereas a new sharp singlet azo methine peak appeared at 8.16 ppm and the aromatic protons were observed near 7.69 to 7.16 ppm in ESI Fig. S6.† A broad singlet peak that appeared at 4.98 ppm was attributed for phenolic proton. In **HL** two singlet methyl protons showed slightly higher field compared to the methyl protons of (**A**). In both the complexes the phenolic proton of **HL** completely disappeared, the azo methine proton

Table 5 Selected optimized geometrical parameters of complexes **1**, **1a** and **1b** in the ground ( $S_0$ ) state at B3LYP levels and experimental bond length (Å) and angle (°)

	$\tau$ (ref. 41) (Zn1)	$\tau$ (ref. 41) (Zn2)	Zn–O <sub>brig</sub> (Å)	Zn–Zn (Å)	O( $\mu$ )–Zn–O( $\mu$ ) (°)	Energy (a.u.)
<b>1</b>	0.15	0.045	2.0405	3.5918	97.18 & 98.54	–5775.17223673
<b>1a</b>	0.63	0.62	2.0022	4.1693	108.11 & 129.75	–5775.16628225
<b>1b</b>	0.068	0.025	2.0615	3.2035	79.42 & 76.68	–5775.15511220



Scheme 3 Jablonski diagram for fluorescence with solvent relaxation.

underwent deshielding field at 8.74 ppm in **1** and 9.07 ppm in **2**, whereas in ligand it appeared at 8.16 ppm. Both these events reveal the indication of complex formation. The methyl proton also shifted in upfield region during complexation near about 2 ppm. The  $^1\text{H}$  NMR spectra of **1** and **2** are depicted in ESI Fig. S7 and S8.†

Complex **1** showed two methyl spectra, one at 2.39 ppm and the other at 2.02 ppm, with the last one showing comparatively lower field region. However, complex **2** depicted only one sharp singlet methyl proton at 2.40 ppm. This observation clearly says that two types of methyl proton exist in complex **1** whereas complex **2** occupied only one type of methyl proton. The peak at 2.40 is attributed for the methyl group present at ligand system and the unique peak at 2.02 ppm in **1** for the methyl proton present at acetate bridge system. This is clear evidence that the di-nuclear and tri-nuclear form of the complex **1** and **2** are present at solid state as well as in solution state also. The correlation between the experimental and calculated  $^1\text{H}$  NMR chemical shift of **1** is shown in Fig. 3 as a representative case.

## IR spectra

The IR spectra of the complexes were recorded in a KBr disk. The calculated IR spectra of all the complexes were reported. The characteristic IR data were given in the Experimental section. In both complexes C–O<sub>phenoxo</sub> stretches were observed at 1220  $\text{cm}^{-1}$  whereas C=N stretches at 1610 and 1605  $\text{cm}^{-1}$  for **1** and **2**, respectively. The characteristic stretching frequency of  $\nu_{\text{as}}(\text{COO}^-)$  and  $\nu_{\text{s}}(\text{COO}^-)$  for **1** were observed at about 1561 and 1363  $\text{cm}^{-1}$ . Both the complexes exhibited broad band at the region of 3500  $\text{cm}^{-1}$  due to aromatic C–H stretching vibrations whereas the band at 2925  $\text{cm}^{-1}$  exhibited asymmetric C<sub>sp<sup>3</sup></sub>H stretching vibrations for methyl group respectively. The bands in the region of 1600–1430  $\text{cm}^{-1}$  were consistent with the skeletal vibration of the aromatic system. The detailed data for IR and NMR spectra are given in Experimental section. The IR spectra of the complexes are given in ESI Fig. S9 and S10.†

## Geometry optimization, structure analysis and different bridging mode of complex **1**

The complexes are diamagnetic at room temperature indicating their singlet ground state  $t_{2g}^6e_g^4$ . The geometry optimization for all the complexes was performed in solution phases in their ground singlet ( $S_0$ ) spin state. The optimized structures of the complexes **1** and **2** at singlet ground state are shown in ESI Fig. S11.† Calculated structures are in excellent agreement with experimental data for the complexes **1** and **2**, for which X-ray data are available. The significant bond distances and angles of the optimized geometry of complex **1** in their singlet ground  $S_0$  state compared with their crystal structure parameter is given in ESI Table S1.† In this complex, the calculated Zn–N and Zn–O bond distances occur near 2.10 and 2.00 Å, respectively which are in very good agreement with the experimental values and the slight discrepancy comes from the crystal lattice distortion existing in real molecules.

The partial frontier molecular orbital compositions and energy levels of **1** in singlet ground state ( $S_0$ ) are listed in Table 4. The partial molecular orbital diagram with some isodensity frontier molecular orbital which are mainly involved in the

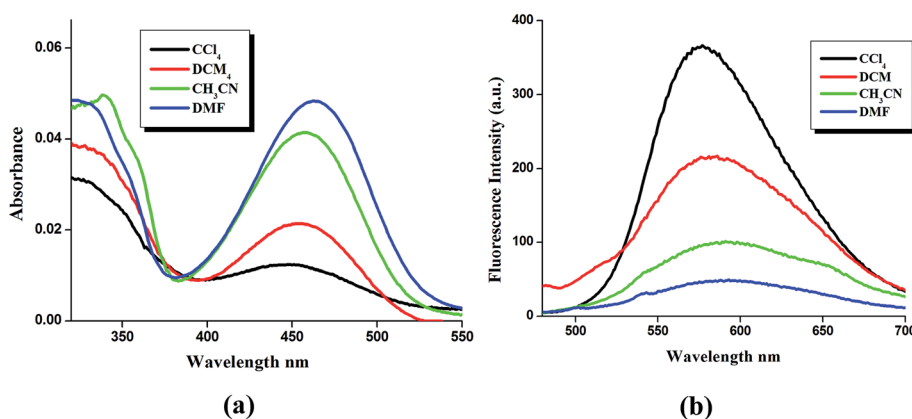


Fig. 5 (a) The absorbance spectra of **1** ( $\sim 1 \times 10^{-5}$  M) in different solvents at room temperature. (b) A representative diagram of emission intensity vs. solvent polarity of the complex **1**.

Table 7 Photophysical parameters of complex **1** in different solvent at room temperature

Solvent	$\lambda_{\text{abs}}$ (nm)	$\lambda_{\text{em}}$ (nm)	Quantum yield ( $\Phi_f$ )	$\tau_1$ (ns)	$\tau_2$ (ns)	$\chi^2$	$k_r \times 10^7$	$k_{\text{nr}} \times 10^8$
CCl <sub>4</sub>	449	577	0.28	0.17	3.96	1.10	7.1	1.81
DCM	453	582	0.21	0.41	4.41	1.22	4.8	1.79
CH <sub>3</sub> CN	458	592	0.10	1.25	5.01	1.40	2.0	1.79
DMF	463	597	0.05	1.20	5.15	1.04	0.9	1.84

electronic transitions for mononuclear complexes **1** and **2** are shown in ESI Fig. S12.† The energy difference between HOMO (H) and LUMO (L) occurs in the 2.63 and 2.56 eV for complex **1** and **2** respectively. The L and L+1 are almost degenerate (energy difference  $\sim 0.24$  eV in **1**,  $\sim 0.06$  eV in **2**). But L+2 is destabilized by an amount  $\sim 0.6$  eV compared to L+1. In dinuclear complexes, the electron density in H and H–1 mainly reside on aldehyde moiety (83%) while in case of H–3 and H–4 the little contribution of electron density arises from acetate bridging group and metal d orbital and the major contribution comes from aldehyde moiety ( $\sim 60\%$ ). L, L+1, L+2 and L+3 of the polynuclear complexes originates from ligand  $\pi^*$  orbital localized on quinoline moiety and aromatic system attached to C=N bond contribution.

Here in we described that the nature of geometry of the complex is influenced by the mode of coordination of oxygen atom in bridging acetate group. We compared optimized geometry between two hypothetical dinuclear complexes  $[\text{Zn}_2(\text{L})_2(\mu^{1,2}\text{-OAc})(\mu^{1,2}\text{-OAc})]$ , **1a** and  $[\text{Zn}_2(\text{L})_2(\mu^{1,1}\text{-OAc})(\mu^{1,1}\text{-OAc})]$ , **1b** with the crystalline form of  $[\text{Zn}_2(\text{L})_2(\mu^{1,2}\text{-OAc})(\mu^{1,1}\text{-OAc})]$ , **1**. It was observed that the naturally selected crystalline complex **1** is more stabilized than the two hypothetical proposed forms

(Fig. 4). In **1b** both the ligand moieties surrounding metal atoms prefer SP geometry, while in case of **1a** it prefers TBP shapes.<sup>41</sup> Hence two metal atoms maintain nearly symmetrical environments towards ligand moiety when the bridging acetate groups used their oxygen atoms to coordinate with the metal in same fashion. On the other hand in **1** the geometry surrounding the metal centre is non symmetric as the coordination modes of bridging atoms are dissymmetric in nature (Table 5).

#### Photophysical study of HL in different solvent

The UV-Vis spectrum of the sensor **HL** was recorded in presence of various types of solvents at room temperature, which displayed a well resolved peak in the range 325 to 350 nm (Fig. S13a†). The fluorophore emits a weak emission band in the region of 420 to 480 nm when excited at 330 nm in presence of different polarity solvent (Fig. S13b†). Both the absorption maxima ( $\lambda_{\text{abs}}$ ) and emission maxima ( $\lambda_{\text{em}}$ ) of this particular fluorophore shifted towards longer wavelength as the polarity of the solvent increases (Table 6).

Table 8 Main calculated optical transition for complex **1** with composition in terms of molecular orbital contribution of the transition, vertical excitation energies and oscillator strength in acetonitrile

Electronic transitions	Composition	Excitation energy	Oscillator strength ( $f$ )	CI	Assign	$\lambda_{\text{exp}}$ (nm)
$S_0 \rightarrow S_1$	H – 1 $\rightarrow$ L	2.6396 eV (463.70 nm)	0.3965	0.17021	<sup>1</sup> ILCT	466
	H $\rightarrow$ L			0.74314	<sup>1</sup> ILCT	
	H $\rightarrow$ L + 1			0.11988	<sup>1</sup> ILCT	
$S_0 \rightarrow S_2$	H – 1 $\rightarrow$ L	2.6741 eV (458.65 nm)	0.0665	0.16688	<sup>1</sup> ILCT	
	H $\rightarrow$ L			–0.68227	<sup>1</sup> ILCT	
	H $\rightarrow$ L + 1			0.19988	<sup>1</sup> ILCT	
$S_0 \rightarrow S_3$	H – 1 $\rightarrow$ L	2.6852 eV (457.72 nm)	0.0372	0.58303	<sup>1</sup> ILCT	
	H $\rightarrow$ L + 1			–0.31162	<sup>1</sup> ILCT	
$S_0 \rightarrow S_{11}$	H – 5 $\rightarrow$ L	3.5506 eV (349.19 nm)	0.2545	–0.15908	<sup>1</sup> MLCT/ <sup>1</sup> ILCT	345
	H – 4 $\rightarrow$ L			–0.23882	<sup>1</sup> MLCT/ <sup>1</sup> ILCT	
	H – 3 $\rightarrow$ L			0.48128	<sup>1</sup> MLCT/ <sup>1</sup> ILCT	
	H – 2 $\rightarrow$ L			–0.33256	<sup>1</sup> ILCT	
	H – 2 $\rightarrow$ L + 1			–0.13673	<sup>1</sup> ILCT	
$S_0 \rightarrow S_{12}$	H – 5 $\rightarrow$ L + 1	3.5736 eV (346.94 nm)	0.2092	–0.13467	<sup>1</sup> MLCT/ <sup>1</sup> ILCT	
	H – 4 $\rightarrow$ L + 1			0.31146	<sup>1</sup> MLCT/ <sup>1</sup> ILCT	
	H – 2 $\rightarrow$ L			0.44082	<sup>1</sup> ILCT	
	H – 2 $\rightarrow$ L + 1			–0.35880	<sup>1</sup> ILCT	
$S_0 \rightarrow S_{13}$	H – 5 $\rightarrow$ L	3.5909 eV (345.28 nm)	0.2790	–0.18707	<sup>1</sup> MLCT/ <sup>1</sup> ILCT	
	H – 4 $\rightarrow$ L + 1			–0.20622	<sup>1</sup> MLCT/ <sup>1</sup> ILCT	
	H – 3 $\rightarrow$ L			0.28261	<sup>1</sup> MLCT/ <sup>1</sup> ILCT	
	H – 2 $\rightarrow$ L			0.41547	<sup>1</sup> ILCT	
	H – 2 $\rightarrow$ L + 1			0.46091		

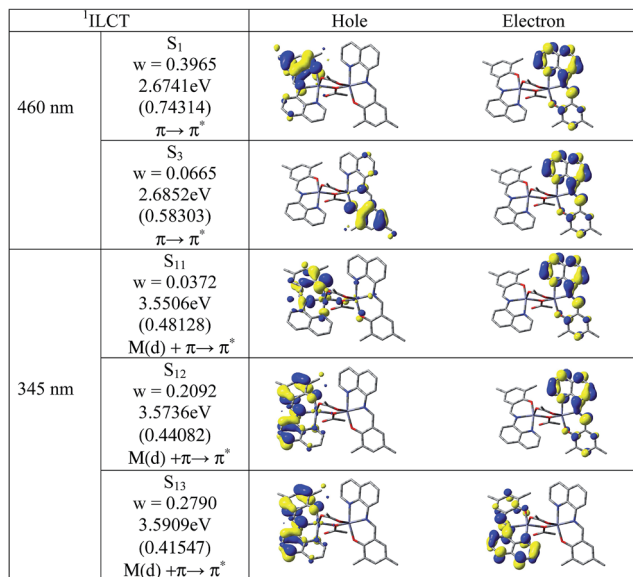


Fig. 6 Natural transition orbitals (NTOs) for the complexes **1** illustrating the nature of optically active singlet excited states in the absorption bands 460 and 345 nm in acetonitrile as a solvent.

Table 9 Main calculated optical transition for complex **1** with composition in terms of molecular orbital contribution of the transition, vertical excitation energies and oscillator strength in solvents of different polarity

Solvent	CCl <sub>4</sub>	DCM	CH <sub>3</sub> CN	DMF
Transition (S <sub>0</sub> → S <sub>1</sub> )	<sup>1</sup> ILCT	<sup>1</sup> ILCT	<sup>1</sup> ILCT	<sup>1</sup> ILCT
Oscillator strength ( <i>f</i> )	0.4356	0.2879	0.3965	0.5013
λ <sub>theo</sub> (nm)	446.01	456.91	463.75	480.61
λ <sub>exp</sub> (nm)	447	454	466	477
Excitation energy (eV)	2.7173	2.6648	2.6390	2.5841

This indicates that the excited state S<sub>1</sub> of the fluorophore is more polar than ground S<sub>0</sub> state.<sup>42</sup> The excess vibrational energy is rapidly lost by the polar solvent molecules and stabilized by

the S<sub>1</sub> state which leads bathochromic shift towards more polar solvent. This typical fluorophore contains the more polar enol form in S<sub>1</sub> state rather than the keto tautomeric form.<sup>6</sup> As a result a larger dipole moment in the excited state ( $\mu_E = 5.2085$  D) was observed than in the ground S<sub>0</sub> state ( $\mu_G = 4.9389$  D). Following excitation the solvent dipoles can reorient or relax around the excited state, which lowers the energy of the S<sub>1</sub> state (Scheme 3).

More structured and intense emission spectra were observed for the fluorophore in the least polar solvent like hexane (Fig. S13b†). As the polarity of the solvent increase the intensity of outcome fluorescence spectra sharply diminishes and broadens (Fig. S13b†). The radiative rate constant (*k<sub>r</sub>*) and non radiative rate constant (*k<sub>nr</sub>*) value were also determined in presence of different polarity solvent (Table 6). It was observed that with increase in dielectric constant decrease in *k<sub>r</sub>* values are more than *k<sub>nr</sub>* (Table 6). The fluorescence life time decay of the ligands was measured in different polarity solvent at 280 nm and the nature of the decay was fitted with mono exponential decay curve (Fig. 10a). The life time ( $\tau$ ) of excited state was more under high polar solvent. The mono exponential emission nature of the fluorophore revealed that the excited state contains only one tautomeric form (enol) in excess.

### Photophysical studies of complexes in different solvent

The absorption spectra of the complexes **1**, **2** and **3** were recorded in different polarity solvent at room temperature. The representative UV-Vis spectra of complex **1** was presented in Fig. 5a, while for the complexes **2** and **3** they were depicted in ESI Fig. S14a and b.† A new band appeared longer wavelength at 450 nm in addition to the ligand characteristic peak around 345 nm. This lower energy characteristic band indicated the complex formation. The absorbance maxima underwent bathochromic shift with increasing dielectric constant of the solvent. The Photophysical data of the complex **1** is given in Table 7, and for complexes **2** and **3** in ESI Tables S2 and S3.†

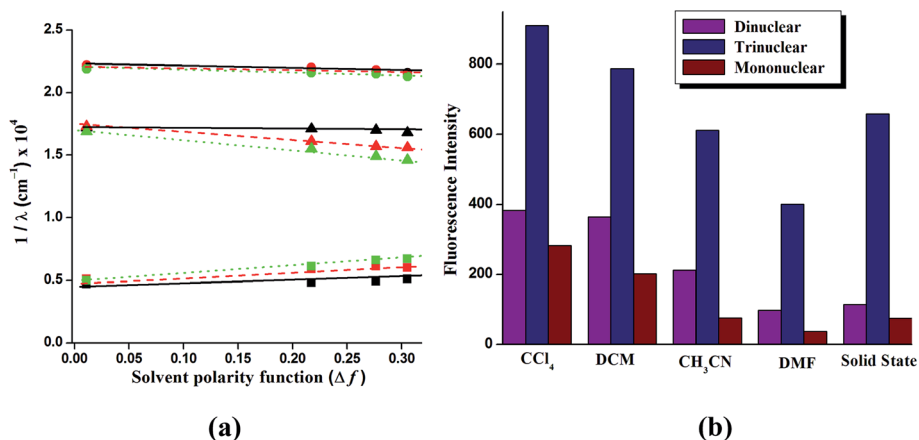
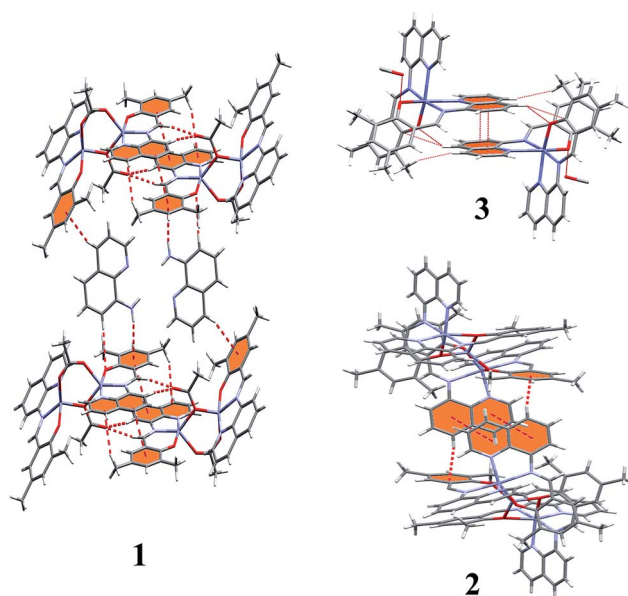


Fig. 7 (a) The black, red and green lines are represented complex **1**, **2** and **3** respectively; from top to bottom the lines are represented the absorption maxima, fluorescence maxima and stokes shifts ( $\bar{\nu}_{\text{abs max}}$ ,  $\bar{\nu}_{\text{fl max}}$  and  $\Delta\bar{\nu}_{\text{Stokes shifts}}$  respectively, in  $\text{cm}^{-1}$ ) of **1**, **2** and **3** against the solvent polarity function,  $\Delta f$ . (b) A bar diagram of fluorescence intensity vs. different medium of the respective complexes was plotted.

Table 10 The C–H⋯π interactions parameters for **1**, **2** and **3**

Y–H( <i>i</i> )⋯Cg( <i>J</i> )	H⋯C(g) (Å)	Y–H⋯C(g) (°)	Y⋯C(g) (Å)	Symmetry
<b>Complex 1</b>				
N(6)–H(6B)⋯Cg(1)	2.71	159	3.525(6)	$-1 + x, 1 + y, z$
C(14)–H(14)⋯Cg(3)	2.96	174	3.888(4)	$x, -1 + y, z$
C(43)–H(43)⋯Cg(4)	2.98	156	3.850(9)	$x, y, z$
<b>Complex 2</b>				
C(27)–H(27A)⋯Cg(1)	2.86	162	3.790(6)	$-x, -y, -z$
C(31)–H(31)⋯Cg(2)	2.54	170	3.456(5)	$1/2 - x, 1/2 - y, 1 - z$
<b>Complex 3</b>				
C(7)–H(6)⋯Cg(8)	2.69	135	3.389(4)	$-x, 1 - y, 1 - z$
C(19)–H(19)⋯Cg(1)	2.90	105	3.284	$x, y, z$

To get better insight on experimental absorption values TDDFT calculations were done for complex **1** on the basis of the optimized geometry. The calculated absorption energies associated with their oscillator strengths, the main configurations and their assignments of **1** is given in Table 8. In order to analyze the nature of absorption, we performed an NTO analysis based on the calculated transition density matrices.<sup>44</sup> Here we referred to the unoccupied and occupied NTOs as “electron” and “hole” transition orbitals, respectively (Fig. 6). Based on our TDDFT NTOs analysis the bands in the region 300–470 nm for this complex can be characterized as an ILCT states. A very little amount of orbital contribution (less than 5%) of metal d-orbital in higher energy transition ( $<S_{10}$ ) was observed. As illustrated in Fig. 6, optical excitations occur from the occupied (hole) transition orbitals to the unoccupied (electron) transition orbitals. Hole NTOs contributing to the bands were localized on the  $\pi$  orbital of ligand while the electron NTOs were mainly delocalized over the  $\pi^*$  orbital of the ligand moiety. The bathochromic shift of the complex **1** in UV-Vis spectrum with increasing solvent polarity was verified by theoretical calculation. We calculated TDDFT and Gausssum2.0 analysis on the basis of the optimized geometry of complex **1** using different polarity solvents. In every case it was observed that the lowest lying distinguishable singlet  $\rightarrow$  singlet absorption band at

Fig. 8 Packing diagram of both the complexes **1**, **2** and **3** with C–H/ $\pi$  and  $\pi$ – $\pi$  stacking interactions.Table 11 The  $\pi$ – $\pi$  stacking interaction parameters for **1**, **2** and **3**<sup>a</sup>

Rings <i>I</i> – <i>J</i>	Cg–Cg (Å)	Cg <sub><i>I</i></sub> _Perp (Å)	Cg <sub><i>J</i></sub> _Perp (Å)	$\alpha$ (°)	Symmetry
<b>Complex 1</b>					
Cg(1)⋯Cg(6)	3.6817(18)	–3.4298(13)	–3.4440(13)	3.25(15)	$2 - x, 1 - y, 1 - z$
<b>Complex 2</b>					
Cg(5)⋯Cg(5)	3.764(2)	–3.3797(17)	–3.3797(17)	0	$1/2 - x, 1/2 - y, 1 - z$
Cg(1)⋯Cg(1)	3.851(3)	–3.6487(18)	–3.6485(18)	14	$1/2 - x, 1/2 - y, 1 - z$
<b>Complex 3</b>					
Cg(5)⋯Cg(5)	3.595(2)	3.3967(15)	3.3967(15)	0	$-x, -y, 1 - z$
Cg(7)⋯Cg(5)	3.624(2)	3.3989(14)	3.3961(14)	2.29(17)	$-x, -y, 1 - z$

<sup>a</sup> Cg(1) = C11/C16, Cg(2) = N1/C9, Cg(3) = N5/C49, Cg(4) = C29/C34, Cg(5) = N4/C36, Cg(6) = C4/C9. Cg(*n*) = ring number;  $\alpha$  = dihedral angle between planes *I* and *J*; Cg–Cg = distance between ring centroids; Cg<sub>*I*</sub>\_Perp = perpendicular distance of Cg(*I*) on ring *J*; Cg<sub>*J*</sub>\_Perp = perpendicular distance of Cg(*J*) on ring *I*.

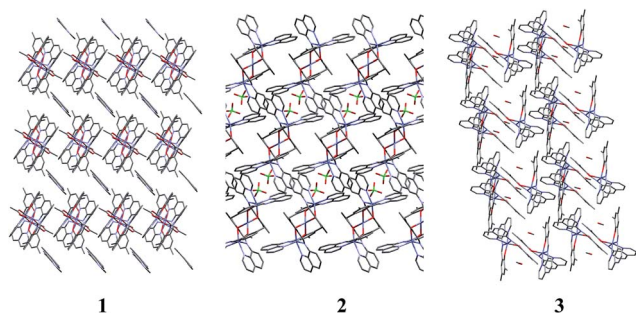


Fig. 9 An extended 2D network perspective view of complexes.

450 nm could be attributed to  $\pi(L) \rightarrow \pi^*(L)$  transitions with ILCT character. It was further observed that the energy gap between HOMO and LUMO in  $S_0 \rightarrow S_1$  transition gradually decreased with increasing solvent polarity (Table 9).

### Emission spectral properties

The emission spectral behaviors of the complexes were studied at room temperature in solvent of different polarity. As shown in Fig. 5b it was observed that the emission intensity gradually decreased with increasing solvent polarity for **1**, while for complexes **2** and **3** they are given in ESI Fig. S15a and b.† We measured the absorption ( $\lambda_{\text{abs max}}$ ) and fluorescence ( $\lambda_{\text{em max}}$ ) band maxima, quantum yield ( $\Phi_f$ ) and lifetime ( $\tau$ ) in different solvents along with the solvent polarity function,  $\Delta f$  (eqn (1))<sup>45</sup>

$$\Delta f = (\varepsilon - 1/2\varepsilon + 1) - (\eta^2 - 1/2\eta^2 + 1) \quad (1)$$

where  $\varepsilon$  and  $\eta$  are the static dielectric constant and refractive index of the solvent, respectively. With increase in solvent polarity, bathochromic shifts in absorbance and emission spectra were observed (Tables 7, S3 and S4†), which revealed that the more polar excited state was stabilized more effectively in solvents of higher polarity.<sup>42</sup> A reasonably good linear fits were obtained when the absorption ( $\bar{\nu}_{\text{abs max}}$ ) or emission

( $\bar{\nu}_{\text{em max}}$ ) band maxima (in  $\text{cm}^{-1}$ ) for **1**, **2** and **3** in different solvents were plotted vs.  $\Delta f$ . The higher slope for the  $\bar{\nu}_{\text{em max}}$  vs.  $\Delta f$  plot as compared to that for the  $\bar{\nu}_{\text{abs max}}$  vs.  $\Delta f$  plot (Fig. 7a) suggested that the excited state of the complexes were more polar than the ground state.<sup>45</sup> To substantiate these results, we also tried to correlate the Stokes' shifts (*i.e.*,  $\Delta\bar{\nu} = \bar{\nu}_{\text{abs}} - \bar{\nu}_{\text{em}}$ ) with the  $\Delta f$  values of the solvents.

The solid state emission was performed for all the complexes. All of them showed a bathochromic shift during excitation at 450 nm. The emission maxima are 550 nm, 554 nm and 572 nm for complex **1**, **2** and **3** respectively, (in ESI Fig. S16†). In the crystal packing, several noncovalent interactions such as hydrogen bonding (ESI Tables S4–S6†), C–H/ $\pi$ ,  $\pi \cdots \pi$  were found. The C–H/ $\pi$  interactions in **1**·C<sub>9</sub>H<sub>8</sub>N<sub>2</sub> were generated by interaction of H6B, H14 and H43 with centroid of the rings Cg(1), Cg(3) and Cg(4) whereas in **2** they are generated by interaction of H27A and H31 with centroid of the rings Cg(1) and Cg(2) and in **3** by interaction of H6 and H19 with centroid of the rings Cg(8) and Cg(1) respectively (Table 10). The  $\pi$ – $\pi$  stacking interaction was found to be involved in aromatic rings with centroid-to-centroid distance minimum for mono nuclear complex (3.595(2) Å, Table 11 and Fig. 8). The face angle ( $\alpha$ ) of zero with minimum distance between two aromatic ring clouds led to larger bathochromic shift rather than for di- and tri- nuclear system. The emission intensity increased gradually from mononuclear to trinuclear (Fig. 7b). A strong  $\pi$ – $\pi$  was involved between two quinoline moieties (Fig. 8) in complex **2** led to more red shifted emission band besides incorporation of non coordinating ammine group which quenched the complex **1** through the PET mechanism taking place in the lone pair of nitrogen atom of free amine.<sup>21</sup> Besides the smaller inter nuclear distance between two Zn atom (3.074 Å), complex **2** underwent spin orbital coupling. On the other hand, similar type interaction did not take place in complex **1** as zinc atoms were far enough (3.599 Å) by acetate bridge than their van der Waal's radius of isolated zinc atom (2.25 Å).<sup>43</sup> Such type of spin orbital interaction somehow enhanced the fluorescence intensity in solid state. An extended 2D network of relevant complexes is given in Fig. 9.

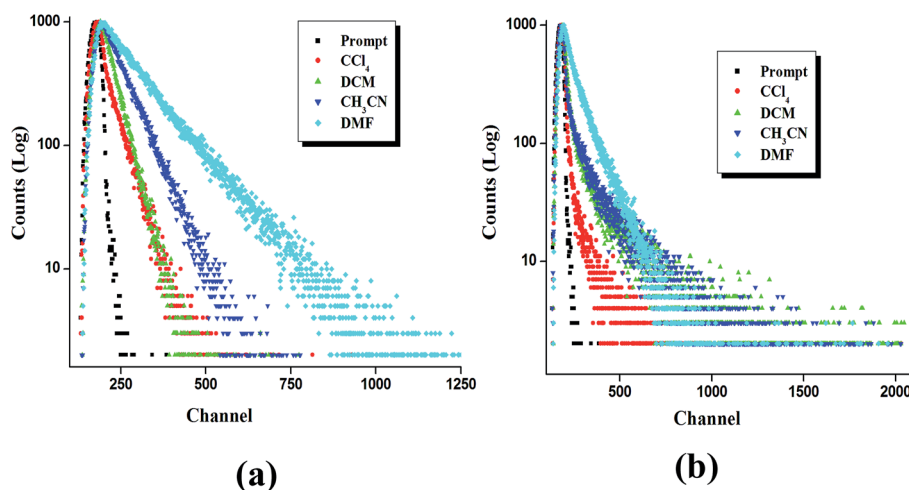


Fig. 10 Changes in the time-resolved photoluminescence decay of HL (a) and **1** (b) in different polarity solvent at room temperature.

Time resolved luminescence spectra proved to be an important tool to understand the decay process and the emissive nature of the complexes in different polarity solvent. All the complexes display a bi-exponential decay nature irrespective of solvent polarity and the decay plot for the complex 1 is shown in Fig. 10b, whereas complexes 2 and 3 are given in ESI Fig. 17a and b.† The value of  $\tau_1$  life time of the complexes was of similar order with the lifetime with ligand which revealed that in excited state the biexponential decay nature of the complexes arise due to the contribution of the ligand moiety as well as the complex itself. The smaller  $k_{nr}$  value (nearly ten times) for the complexes compared to that of the isolated ligand suggested the enhancement of fluorescence intensity due to complexation.

## Conclusion

So as a whole we have synthesized three zinc complexes containing Schiff base with different stoichiometric ratio and its photo physics has been characterized by absorption, emission, time-resolved emission spectroscopic techniques as well as by theoretical study. The highest emission intensity was observed in trinuclear complex. In summary we conclude that the incorporation of more zinc atom during complexation leads to stronger fluorescence intensity with gradually bathochromic shift in solution of different polarity. The solvent polarity function plot shows that excited state of the complexes are more polar than the ground state. Moreover, it shows a regular increasing trade of life time ( $\tau_2$ ) as the polarity of investigated solvent is increased. The quantum yield as well as radiative rate constant ( $k_r$ ) value is significantly monitored by solvent polarity while the non radiative rate constant values ( $k_{nr}$ ) remain almost constant in the complexes.

## Acknowledgements

Amar Hens acknowledge UGC, New Delhi for the research fellowship. We are also thankful to Department of Science and Technology (DST), New Delhi, India for the data collection on the CCD facility setup (Jadavpur University) under DST-FIST program. We also acknowledge CAS, Department of Chemistry, Jadavpur University and DST-PURSE program for other facilities. The author acknowledges Ashok Sasmal of Jadavpur University, for help in weak interaction calculation.

## References

- M. Maiti, D. Sadhukhan, S. Thakurta, S. Roy, G. Pilet, R. J. Butcher, A. Nonat, L. J. Charbonnière and S. Mitra, *Inorg. Chem.*, 2008, **51**, 12176–12187.
- S. Sen, P. Talukder, S. K. Dey, S. Mitra, G. Rosair, D. L. Hughes, G. P. A. Yap, G. G. Pilet, V. Gramlich and T. Matsushita, *Dalton Trans.*, 2006, 1758–1767.
- P. Bhattacharya, J. Parr and A. T. Ross, *J. Chem. Soc., Dalton Trans.*, 1998, 3149–3150.
- R. T. Ruck and E. N. Jacobsen, *J. Am. Chem. Soc.*, 2002, **124**, 2882–2883.
- D. M. Epstein, S. Choudhary, M. R. Churchill, K. M. Keil, A. V. Eliseev and J. R. Morrow, *Inorg. Chem.*, 2001, **40**, 1591–1596.
- A. Hens, P. Mondal and K. K. Rajak, *Dalton Trans.*, 2013, 14905–14915.
- C. Dhenaut, I. Ledoux, I. D. W. Samuel, J. Zyss, M. Bourgault and H. Le Bozec, *Nature*, 1995, **374**, 339–342.
- (a) M. Bourgault, K. Baum, H. Le Bozec, G. Pucetti, I. Ledoux and J. Zyss, *New J. Chem.*, 1998, 517–522; (b) T. Renouard, H. Le Bozec, S. Brasselet, I. Ledoux and J. Zyss, *Chem. Commun.*, 1999, 871–872.
- K. Senechal, O. Maury, H. Le Bozec, I. Ledoux and J. Zyss, *J. Am. Chem. Soc.*, 2002, **124**, 4560–4561.
- P. Wang, C. Klein, R. Humphry-Baker, S. M. Zakeeruddin and M. Gratzel, *J. Am. Chem. Soc.*, 2005, **127**, 808–809.
- S. R. Jang, C. Lee, H. Choi, J. J. Ko, J. Lee, R. Vittal and K. J. Kim, *Chem. Mater.*, 2006, **18**, 5604–5608.
- L. X. Chen, W. J. H. Jager, D. J. Gosztola, M. P. Niemczyk and M. R. Wasielewski, *J. Phys. Chem. B*, 1997, **104**, 1950–1960.
- A. Ajayaghosh, P. Carol and S. Sreejith, *J. Am. Chem. Soc.*, 2005, **127**, 14962–14963.
- A. E. Dennis and R. C. Smith, *Chem. Commun.*, 2007, 4641–4643.
- D. C. Freeman and C. E. White, *J. Am. Chem. Soc.*, 1956, **78**, 2678–2682.
- C. E. White and F. Cuttitta, *Anal. Chem.*, 1959, **31**, 2083–2087.
- R. M. Dagnall, R. Smith and T. S. West, *J. Chem. Soc. A*, 1966, 1595–1598.
- Y. Hamada, T. Sano, M. Fujita, T. Fujii, Y. Nishio and K. Shibata, *Jpn. J. Appl. Phys., Part 2*, 1993, **32**, L511–L513.
- T. Sano, Y. Nishio, Y. Hamada, H. Takahashi, T. Usuki and K. Shibata, *J. Mater. Chem.*, 2000, **10**, 157–161.
- (a) M. Shimizu and T. Hiyama, Organic Fluorophores Exhibiting Highly Efficient Photoluminescence in the Solid State, *Chem.–Asian J.*, 2010, **5**, 1516–1531; (b) K. T. Kamtekar, A. P. Monkman and M. R. Bryce, Recent Advances in White Organic Light-Emitting Materials and Devices (WOLEDs), *Adv. Mater.*, 2010, **22**, 572–582.
- (a) S. S. Sun, J. A. Anspach, A. J. Lees and P. Y. Zavalij, *Organometallics*, 2002, **21**, 685–693; (b) F. Y. Wu, Z. Li, L. Guo, X. Wang, M. H. Lin, Y. F. Zhao and Y. B. Jiang, *Org. Biomol. Chem.*, 2006, **4**, 624–630; (c) D. Das, B. G. Chand, K. K. Sarker, J. Dinda and C. Sinha, *Polyhedron*, 2006, **25**, 2333–2340; (d) V. Luxami and S. Kumar, *RSC Adv.*, 2012, **2**, 8734–8740.
- G.-X. Liu, Y.-Y. Xu, Y. Wang, S. Nishihara and X.-M. Ren, *Inorg. Chim. Acta*, 2010, **363**, 3932–3938.
- (a) A. Sarkar, A. K. Ghosh, V. Bertolasi and D. Ray, *Dalton Trans.*, 2012, 1889–1896; (b) L. J. Daumann, K. E. Dalle, G. Schenk, R. P. McGeary, P. V. Bernhardt, D. L. Ollis and L. R. Gahan, *Dalton Trans.*, 2012, 1695–1708; (c) Z. Xu, J. Yoon and D. R. Spring, *Chem. Soc. Rev.*, 2010, **39**, 1996–2006.
- (a) G. Masanta, C. S. Lim, H. J. Kim, J. H. Han, H. M. Kim and B. R. Cho, *J. Am. Chem. Soc.*, 2011, **133**, 5698–5700; (b) H.-Y. Lin, P.-Y. Cheng, C.-F. Wan and A.-T. Wu, *Analyst*, 2012, **137**, 4415–4417; (c) Y. Mikata, A. Yamashita,

- A. Kawamura, H. Konno, Y. Miyamoto and S. Tamotsu, *Dalton Trans.*, 2009, 3800–3806.
- 25 (a) K. Wolinski, J. F. Hinton and P. Pulay, *J. Am. Chem. Soc.*, 1990, **112**, 8251–8260; (b) P. Tahtinen, A. Bagno, K. Klika and K. Pihlaja, *J. Am. Chem. Soc.*, 2003, **125**, 4609–4618; (c) F. Cloran, I. Carmichael and A. S. Serianni, *J. Am. Chem. Soc.*, 2001, **123**, 4781–4791.
- 26 (a) P. Mondal, A. Hens, S. Basak and K. K. Rajak, *Dalton Trans.*, 2013, 1536–1549; (b) B. Valuer, *Molecular Fluorescence: Principle and Applications*, Wiley-BCH, Weinheim, 2001.
- 27 E. Runge and E. K. U. Gross, *Phys. Rev. Lett.*, 1984, **52**, 997–1000.
- 28 (a) A. D. Becke, *J. Chem. Phys.*, 1993, **98**, 5648–5652; (b) C. Lee, W. Yang and R. G. Parr, *Phys. Rev. B: Condens. Matter Mater. Phys.*, 1988, **37**, 785–789.
- 29 (a) M. E. Casida, C. Jamoroski, K. C. Casida and D. R. Salahub, *J. Chem. Phys.*, 1998, **108**, 4439–4449; (b) R. E. Stratmann, G. E. Scuseria and M. J. Frisch, *J. Chem. Phys.*, 1998, **109**, 8218–8224; (c) R. Bauernschmitt and R. Ahlrichs, *Chem. Phys. Lett.*, 1996, **256**, 454–464.
- 30 (a) V. Barone and M. Cossi, *J. Phys. Chem. A*, 1998, **102**, 1995–2001; (b) M. Cossi and V. Barone, *J. Chem. Phys.*, 2001, **115**, 4708–4717; (c) M. Cossi, N. Rega, G. Scalmani and V. Barone, *J. Comput. Chem.*, 2003, **24**, 669–681.
- 31 (a) T. Liu, H.-X. Zhang and B.-H. Xia, *J. Phys. Chem. A*, 2007, **111**, 8724–8730; (b) X. Zhou, H.-X. Zhang, Q.-J. Pan, B.-H. Xia and A.-C. Tang, *J. Phys. Chem. A*, 2005, **109**, 8809–8818; (c) X. Zhou, A.-M. Ren and J.-K. Feng, *J. Organomet. Chem.*, 2005, **690**, 338–347; (d) A. Albertino, C. Garino, S. Ghiani, R. Gobetto, C. Nervi, L. Salassa, E. Rosenverg, A. Sharmin, G. Viscardi, R. Buscaino, G. Cross and M. Milanesio, *J. Organomet. Chem.*, 2007, **692**, 1377–1391.
- 32 P. J. Hay and W. R. Wadt, *J. Chem. Phys.*, 1985, **82**, 299–310.
- 33 M. J. Frisch, G. W. Trucks, H. B. Schlegel, G. E. Scuseria, M. A. Robb, J. R. Cheeseman, G. Scalmani, V. Barone, B. Mennucci, G. A. Petersson, H. Nakatsuji, M. Caricato, X. Li, H. P. Hratchian, A. F. Izmaylov, J. Bloino, G. Zheng, J. L. Sonnenberg, M. Hada, M. Ehara, K. Toyota, R. Fukuda, J. Hasegawa, M. Ishida, T. Nakajima, Y. Honda, O. Kitao, H. Nakai, T. Vreven, J. A. Montgomery Jr, J. E. Peralta, F. Ogliaro, M. Bearpark, J. J. Heyd, E. Brothers, K. N. Kudin, V. N. Staroverov, R. Kobayashi, J. Normand, K. Raghavachari, A. Rendell, J. C. Burant, S. S. Iyengar, J. Tomasi, M. Cossi, N. Rega, J. M. Millam, M. Klene, J. E. Knox, J. B. Cross, V. Bakken, C. Adamo, J. Jaramillo, R. Gomperts, R. E. Stratmann, O. Yazyev, A. J. Austin, R. Cammi, C. Pomelli, J. W. Ochterski, R. L. Martin, K. Morokuma, V. G. Zakrzewski, G. A. Voth, P. Salvador, J. J. Dannenberg, S. Dapprich, A. D. Daniels, Ö. Farkas, J. B. Foresman, J. V. Ortiz, J. Cioslowski and D. J. Fox, *Gaussian 09, (Revision A.1)*, Gaussian, Inc., Wallingford, CT, 2009.
- 34 (a) N. M. O'Boyle, A. L. Tenderholt and K. M. Langner, *J. Comput. Chem.*, 2008, **29**, 839–845; (b) J. W. Geary, *Coord. Chem. Rev.*, 1971, **7**, 81–122.
- 35 (a) K. Wolinski, J. F. Hilton and P. Pulay, *J. Am. Chem. Soc.*, 1990, **112**, 8251–8260; (b) R. Ditchfield, *Mol. Phys.*, 1974, **27**, 789–807; (c) R. Mcweeny, *Phys. Rev.*, 1962, **126**, 1028–1034; (d) F. London, *J. Phys. Chem.*, 1937, 397–409.
- 36 (a) C. M. Rohlfing, L. C. Allen and R. Ditchfield, *Chem. Phys.*, 1984, **87**, 9–15; (b) M. Cossi, V. Barone, B. Mennucci and J. Tomasi, *Chem. Phys. Lett.*, 1998, **286**, 253–260; (c) E. Cancès, B. Mennucci and J. Tomasi, *J. Chem. Phys.*, 1997, **107**, 3032–3041.
- 37 *SMART; SAINT; SADABS; XPREP; SHELXTL*, Bruker AXS Inc., Madison, WI, 1998.
- 38 G. M. Sheldrick, *SHELXTL*, v. 6.14, Bruker AXS Inc., Madison, WI, 2003.
- 39 (a) C. K. Johnson, *ORTEP Report ORNL-5138*, Oak Ridge National Laboratory, Oak Ridge, TN, 1976; (b) C. F. Macrae, P. R. Edgington, P. McCabe, E. Pidcock, G. P. Shields, R. Taylor, M. Towler and J. van de Streek, *J. Appl. Crystallogr.*, 2006, **39**, 453–457.
- 40 J. W. Geary, *Coord. Chem. Rev.*, 1971, **7**, 81–122.
- 41 C. O'Sullivan, G. Murphy, B. Murphy and B. Hathaway, *J. Chem. Soc., Dalton Trans.*, 1999, 1835–1844.
- 42 S. Nad, M. Kumbhakar and H. Pal, *J. Phys. Chem. A*, 2003, **107**, 4808–4816.
- 43 S. S. Bastanov, *Inorg. Mater.*, 2001, **37**, 871–885.
- 44 R. L. Martin, *J. Chem. Phys.*, 2003, **118**, 4775–4777.
- 45 P. Mahato, S. Saha and A. Das, *J. Phys. Chem. C*, 2012, **116**, 17448–17457.